PHYSICS AND CHEMISTRY OF SOLID STATE
V. 25, No. 2 (2024) pp. 325-332
Section: Chemistry

DOI: 10.15330/pcss.25.2.325-332

Vasyl Stefanyk Precarpathian National University

ФІЗИКА І ХІМІЯ ТВЕРДОГО ТІЛА
Т. 25, № 2 (2024) С. 325-332
Хімічні науки

UDC 546+544.6

ISSN 1729-4428 (Print)
ISSN 2309-8589 (Online)

V. Kordan[1], V. Nytka[1], I. Tarasiuk[1], K. Kluziak[2], V. Pavlyuk[1,2]

Synthesis and electrochemical hydrogenation of $R_xTb_{2-x}Ni_{17}$ and $Tb_2Ni_{17-y}M_y$ phases (R = Y, Zr, La; M = Li, Mg)

[1]*Ivan Franko National University of Lviv, Lviv, Ukraine,*
[2]*Jan Długosz University of Czestochowa, Czestochowa, Poland, vasyl.kordan@lnu.edu.ua*

Alloys from the regions of existence of the solid solutions $R_xTb_{2-x}Ni_{17}$ and $Tb_2Ni_{17-y}M_y$ were synthesized by arc-melting with further annealing at 400 ºC. Quantitative and qualitative composition of alloys and powders of electrode materials was determined by scanning electron microscopy and energy-dispersive X-ray spectroscopy. The Tb/*R*/Ni and Tb/Ni/Mg ratio in the samples was confirmed also by X-ray fluorescence spectroscopy. The cell parameters of $R_xTb_{2-x}Ni_{17}$ (x = 0.5) ternary phases are: a = 8.2987(9) Å, c = 8.0206(8) Å, V = 478.37(9) Å^3 for R = Zr, a = 8.3161(6) Å, c = 8.0482(8) Å, V = 482.03(6) Å^3 for R = Y and a = 8.3690(6) Å, c = 8.0560(7) Å, V = 488.66(6) Å^3 for R = La. Tb atoms were partially substituted by Y, Zr and La atoms because of closeness of atomic radii size. Under experimental condition capacity parameters were 1.81 H/f.u. for the Zr-containing electrode, 2.29 H/f.u. for the Y-containing electrode and 2.31 H/f.u. for the La-containing electrode. In the case of Li,Mg co-doped electrodes we observed more than 2.5 H/f.u. Cell parameters of the Zr- and La-containing phases after hydrogenation increased isotropically. Synthesized hydrides can be interpreted as superstructures with the $Tb_2Mn_{17}C_{2.5}$-type (filled-up of Th_2Ni_{17}). The $Y_{0.5}Tb_{1.5}Ni_{17}$-based electrode demonstrates the potential corrosion at -0.540 V, electrodes with the compositions $Zr_{0.5}Tb_{1.5}Ni_{17}$ and $La_{0.5}Tb_{1.5}Ni_{17}$ show -0.413 V and -0.405 V, respectively. Li and Mg-codoped electrodes shoved the corrosion potential -0.410 V ($Tb_2Ni_{16.4}Li_{0.2}Mg_{0.4}$) and -0.550 V for $Tb_2Ni_{15.6}Li_{0.6}Mg_{0.8}$, respectively.

Keywords: powder X-ray diffraction; scanning electron microscopy; Th_2Ni_{17}-type structure; electrochemical properties; Ni-MH battery.

Received 26 November 2023; Accepted 9 May 2024.

Introduction

Hydrogen energy and hydrogen accumulation are the most promising objects in the modern industry. Materials for hydrogen accumulation in the form of hydrides of metals, intermetallic compounds or composites are attractive and perspective. These materials have different crystal structures and compositions, for example $CaCu_5$ [1–7], $MgCu_2$ [8], $MgZn_2$, $MgNi_2$, Ce_2Ni_7 [9–11] Gd_2Co_7, Th_2Ni_{17}, Th_2Zn_{17} [12] and their derivatives. The results of metallic Mg-based electrode doping with Li and Al are presented in Ref. [13, 14]. Hydrogen absorption ability of the phases and composites with high content of Mg was discussed in Ref. [15–18]. Based on the La_2Mg_{17} compound composite alloys with addition of the $LaNi_5$ compound show an increase of the hydrogenation rate about 3–4 times and a decrease of activation energy during the gas hydrogenation [15]. Related to the Th_2Ni_{17}-type structure new superstructures $La_{3.65}Mg_{30}Sn_{1.10}$ [16] and $La_{3.65}Mg_{30}Sb_{1.07}$ [17] were found and discussed.

Isnard et al. [19] investigated several deuterides $R_2Fe_{17}D_x$ by neutron diffraction and found that for hydrogen the octahedral site in Wyckoff position 6*h* is favored in the hydrides and deuterides. At H content $x > 3$ only substantial occupation of the tetrahedral site in Wyckoff position 12*i* is occurred. Neutron studies [19, 20] are the most precise for determining the position of hydrogen or deuterium in compounds. This is necessary for structural or component modification of alloys to increase sorption capacity or corrosion resistance. During the electrochemical process of charge carriers

intercalation, the interaction of electrolyte components with the electrode surface affects negatively the electrochemical parameters of the battery. An electrode material must be inert to the influence of the electrolyte, so that the surface passivation is minimal, for example during the intercalation of lithium into the orthorhombic perovskite structure [21, 22].

The aim of our work was to synthesize alloys $R_{2.6}Tb_{7.9}Ni_{89.5}$ (R = Y, Zr, La) and Li,Mg co-doped Tb_2Ni_{17} to determine the effect of *d*-elements and *s*-elements doping on electrochemical and hydrogen sorption properties of the Tb_2Ni_{17} binary phase.

I. Materials and experimental methods

Terbium, nickel, lanthanum, yttrium, magnesium with nominal purities of more than 99.99 wt.%, zirconium with nominal purity of more than 99.999 wt.%, and lithium 99.9 wt.% were used as the starting materials. Ingots of alloys were synthesized by arc-melting of mixture of pure elements (5-% excess of Li and Mg) under purified argon atmosphere. Difference between the mass of pure components and the mass of the alloys was measured, the loss during melting did not exceed 2 wt. %. Homogenizing annealing was performed at a temperature of 400 ºC for 30 days in evacuated quartz ampoules with further quenching in cold water without breaking the ampoules.

The efficiency of the electrochemical hydrogenation was investigated in two- and three-electrode Swagelok-type cells. A synthesized powdered alloy was used as anode material. It was mixed with the electrolyte (6M KOH solution). An electrolyte-soaked mixture (9:1) of nickel (II) hydroxide (prepared from $NiSO_4 \cdot 7H_2O$ (99 wt. %) and KOH (98 wt. %)) and graphite (commercial) was used as the cathode material. Electrochemical measurements were carried out in the galvanostatic mode at 1.0 mA/cm^2 using MTech G410-2 galvanostat [23]. Cyclic voltammetry and electrochemical impedance spectroscopy were carried out using 3-electrode "Swagelok-type" cell and potentiostate-galvanostat from CH Instruments (Austin, TX, USA). The $Ni(OH)_2$ or Hg/HgO was used as a reference electrode. Potential scan rate from the cathodic towards the anodic direction was 10 mV/sec.

Diffraction data were obtained on DRON-2.0M powder diffractometer (Fe K_α – radiation). The experimental diffraction patterns of alloys were compared with the theoretical Tb_2Ni_{17} diffraction pattern, calculated in the program Powder Cell [24]. Unit cell parameters were determined using programs LATCON [25] and FullProf [26]. The quantitative and qualitative compositions of studied samples were investigated using energy-dispersive X-ray spectroscopy (Tescan Vega3 LMU scanning electron microscope (SEM) with Oxford Instruments Aztec ONE System and electron microscope REMMA-102-02 with an elemental microanalyzer) and X-ray fluorescence spectroscopy (ElvaX Pro X-ray fluorescence analyzer). SEM-images and energy-dispersive X-ray analysis (EDX) results were obtained at 20-25 kV voltage and high vacuum atmosphere ($9.0 \cdot 10^{-3}$ Pa). X-ray fluorescence spectra were obtained at 60 kV Rh-tube source.

II. Results and discussion

To investigate the doping of elements (Y, Zr, La) influence on the hydrogen sorption properties and corrosion stability of the Tb_2Ni_{17} binary intermetallic compound, we prepared a three ternary samples $Y_{2.6}Tb_{7.9}Ni_{89.5}$, $Zr_{2.6}Tb_{7.9}Ni_{89.5}$, and $La_{2.6}Tb_{7.9}Ni_{89.5}$. XRD phase analysis showed that all samples contain the hexagonal phase with the Th_2Ni_{17}-type (space group $P6_3/mmc$, Pearson symbol $hP38$) as a main phase. Nickel or based on Ni the $Ni_{1-x-y}R_xTb_y$ solid solution is the minor phase, which is in good agreement with the Tb–Ni phase diagram. Cell parameters for studied ternary phases are presented in Table. The volume of unit cell correlated well with atomic radii of *R*-doping components (r_Y = 1.79 Å, r_{Zr} = 1.62 Å, r_{La} = 1.87 Å). SEM-images of powdered samples before and after hydrogenation are presented in Fig. 1. After electrochemical processes the size of the electrode grains significantly decreased from 5-10 μm to 1-5 μm. EDX-analysis confirmed the formation of 2:17 stoichiometry phases in prepared alloys. After hydrogenation, the integral composition of the powders practically does not differ from the initial one. Small dark areas after hydrogenation are explained by surface etching and adsorption of electrolyte components, for example KOH (after contact with air K_2CO_3 is formed). X-ray fluorescence spectra of the electrode samples (Fig. 2) also confirm the stability of composition of the electrodes after electrochemical processes in alkaline solution (6 M KOH).

SEM-image of the $Y_{2.6}Tb_{7.9}Ni_{89.5}$ alloy and elemental mapping are presented in Fig. 3. Integral composition $Y_{2.6}Tb_{7.6}Ni_{89.8}$ correlates well with nominal composition. The alloy contains the main phase with the stoichiometry 2:17 ($Y_{2.8(7)}Tb_{8.5(5)}Ni_{88.7(6)}$) and the Ni-based minor phase ($Y_{1.1(8)}Tb_{3.7(6)}Ni_{95.2(6)}$). Powder XRD patterns of the $Y_{2.6}Tb_{7.9}Ni_{89.5}$ sample before and after 50 cycles of hydrogenation/dehydrogenation are shown in Fig. 4.

We performed electrochemical hydrogenation of the $R_xTb_{2-x}Ni_{17}$ alloys from the region of solid solution existence. Selected discharge curves at galvanostatic mode (1.0 mA/cm^2) are presented in Fig. 5. Under experimental condition capacity parameters are 1.81 H/f.u. for the Zr-containing electrode, 2.29 H/f.u. for the Y-containing electrode and 2.31 for the La-containing electrode. These values of discharge capacity are not more than 45–50 mA·h/g, but they show the influence of alloying component on electrochemical characteristics. Discharge capacity depends on crystal structure (cell volume, void size) and electrochemical behaviour of components (related to the hydrogen, corrosion activity). The dehydrogenation process occurs at the values of the discharge plateau potential of 1.40–1.10 V. We assumed that by gas hydrogenation at high pressure we can obtain the hydrides $R_2M_{17}H_4$ with larger content of hydrogen. The value 4–4.5 H/f.u is equal to the discharge capacity of 90–100 mA·h/g. The main advantage of 2:17 stoichiometry electrodes is low content of rare-earth elements, which will affect the price of commercial battery.

Corrosion stability of electrodes was studied using cyclic voltammetry. All samples demonstrated stability in the range of potential from -0.4 to +0.4 V. In the case of

Table 1.

Unit cell parameters of the $R_xTb_{2-x}Ni_{17}$ and $Tb_2Ni_{17-y}M_y$ phases

Composition of electrode	Before hydrogenation			After hydrogenation		
	a, Å	*c*, Å	*V*, Å^3	*a*, Å	*c*, Å	*V*, Å^3
$Zr_{2.6}Tb_{7.9}Ni_{89.5}$	8.2987(9)	8.0206(8)	478.37(9)	8.3366(9)	8.0267(9)	483.10(9)
$La_{2.6}Tb_{7.9}Ni_{89.5}$	8.3690(6)	8.0560(7)	488.66(6)	8.421(1)	8.092(1)	497.0(1)
$Y_{2.6}Tb_{7.9}Ni_{89.5}$	8.3161(6)	8.0482(8)	482.03(6)	8.3712(7)	8.0353(9)	487.66(7)
[27]$Tb_{10.5}Ni_{84.0}Li_{2.2}Mg_{3.3}$	8.3115(2)	8.0286(3)	480.32(2)	8.344(1)	8.051(2)	485.5(1)
[27]$Tb_{10.5}Ni_{81.8}Li_{3.3}Mg_{4.4}$	8.3129(4)	8.0384(4)	481.08(4)	8.3488(5)	8.0593(6)	486.49(6)

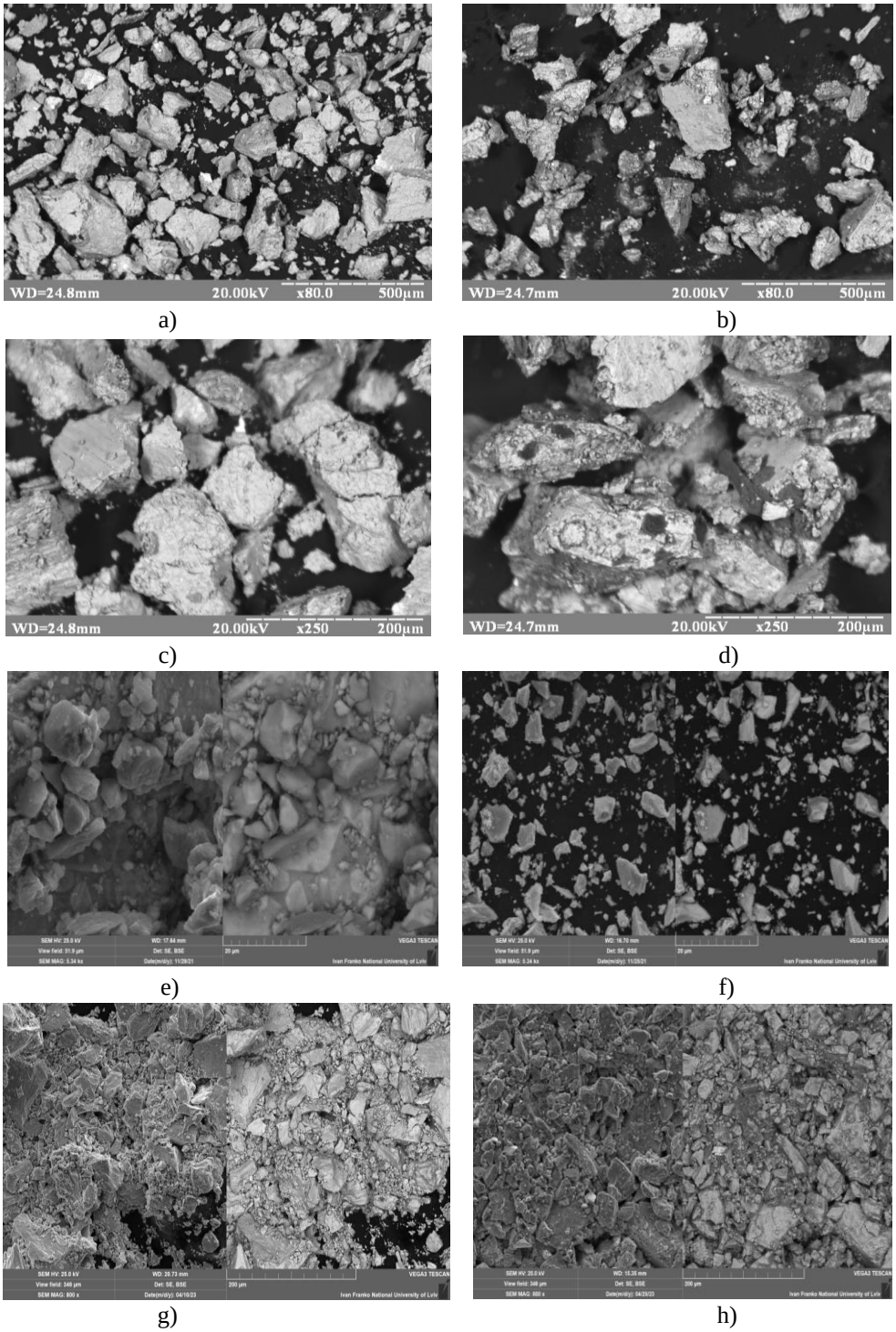

Fig. 1. SEM-images of the electrode materials based on $Zr_xTb_{2-x}Ni_{17}$ (before 50 cycles of the hydrogenation process – $Zr_{0.4}Tb_{1.7}Ni_{16.9}$ (*a*), after – $Zr_{0.5}Tb_{1.6}Ni_{16.9}$ (*b*)), $La_xTb_{2-x}Ni_{17}$ (before– $La_{0.6}Tb_{1.4}Ni_{17.0}$ (*c*), after – $La_{0.5}Tb_{1.4}Ni_{17.1}$ (*d*)), $Y_xTb_{2-x}Ni_{17}$ (before – $Y_{0.5}Tb_{1.5}Ni_{17.0}$ (*e*), after – $Y_{0.4}Tb_{1.5}Ni_{17.1}$ (*f*)) and $Tb_2Ni_{17-x-y}Li_xMg_y$ (before – $Tb_{1.9}Ni_{16.5}Mg_{0.6}$(*g*)), (after – $Tb_{1.8}Ni_{16.5}Mg_{0.7}$ (*h*)).

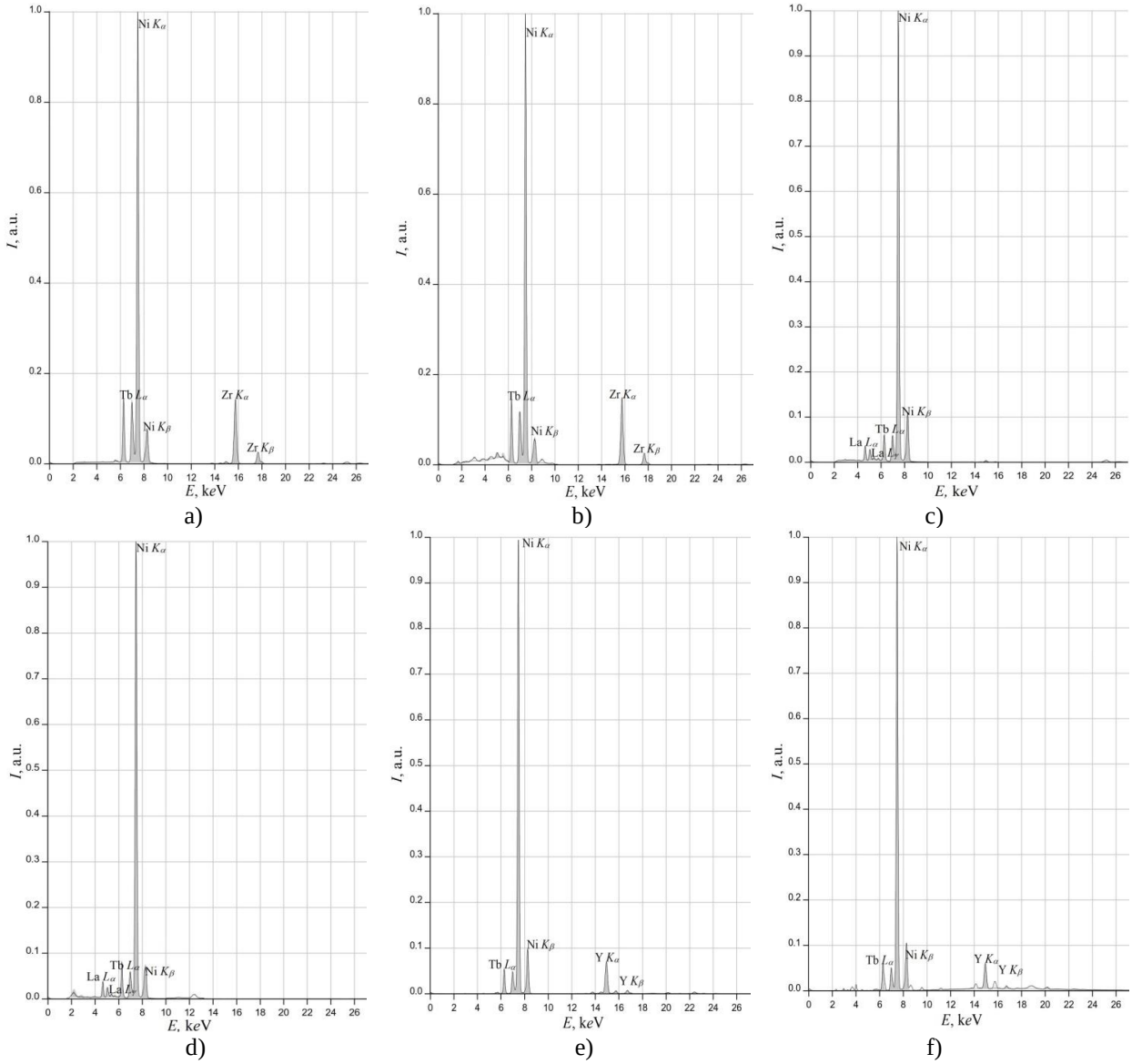

Fig. 2. X-ray fluorescence spectra of the electrode samples: (*a*) before hydrogenation – $Zr_{2.5}Tb_{8.2}Ni_{89.3}$, (*b*) after hydrogenation – $Zr_{.8}Tb_{7.7}Ni_{89.5}$, (*c*) before hydrogenation – $La_{2.7}Tb_{8.3}Ni_{89.0}$, (*d*) after hydrogenation – $La_{3.3}Tb_{7.0}Ni_{89.7}$, (*e*) before hydrogenation – $Y_{3.1}Tb_{9.0}Ni_{87.9}$, (*f*) after hydrogenation – $Y_{3.1}Tb_{9.0}Ni_{87.9}$.

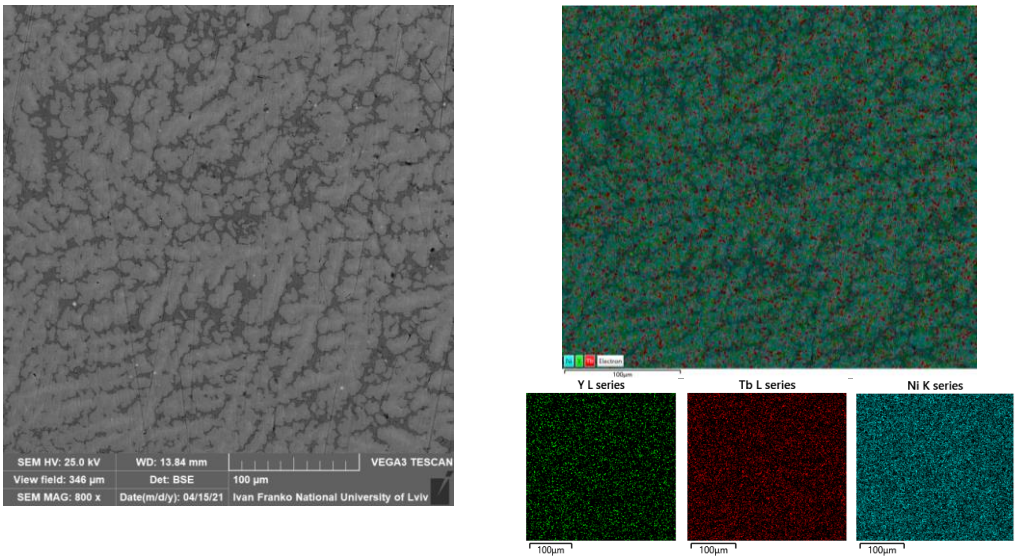

Fig. 3. SEM-image and elemental distribution on the surface of the $Y_{2.6}Tb_{7.9}Ni_{89.5}$ alloy (integral composition – $Y_{2.6}Tb_{7.6}Ni_{89.8}$,main phase – $Y_{2.8(7)}Tb_{8.5(5)}Ni_{88.7(6)}$, dark phase – $Y_{1.1(8)}Tb_{3.7(6)}Ni_{95.2(6)}$).

the Zr-containing electrode we observed the oxidizing anodic processes at potential > 1.0 V. Dynamic polarization curves were obtained by logarithmization of current of the first cycle of voltammetry. Cyclic voltammetry and dynamic polarization curves for the $R_xTb_{2-x}Ni_{17}$-based electrodes are presented in Fig. 6. The best corrosion stability was observed for the $Y_{0.5}Tb_{1.5}Ni_{17}$ alloy (potential corrosion is -0.540 V). The Zr- and La-containing electrodes showed -0.413 V and -0.405 V, respectively.

Nyquist diagrams (imagine resistance as function of real resistance, $-Z = f(Z)$) of studied electrodes are

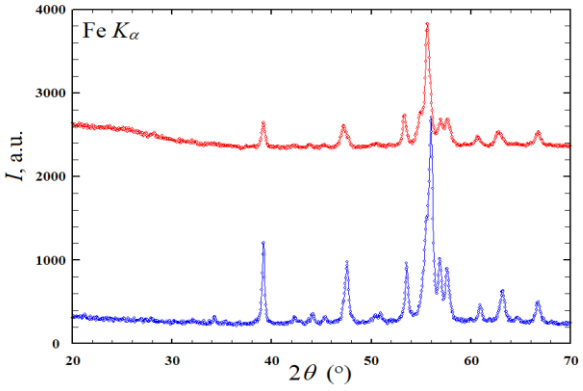

Fig. 4. X-ray powder patterns of the $Y_{0.5}Tb_{1.5}Ni_{17}$ before (bottom) and after (top) 50 cycles of hydrogenation/dehydrogenation.

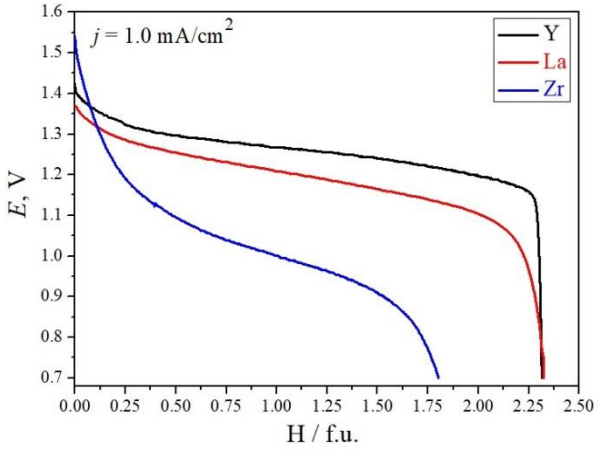

Fig. 5. Selected discharge curves (10-th cycle) for the Ni-MH battery prototype with the $R_xTb_{2-x}Ni_{17}$-based electrodes.

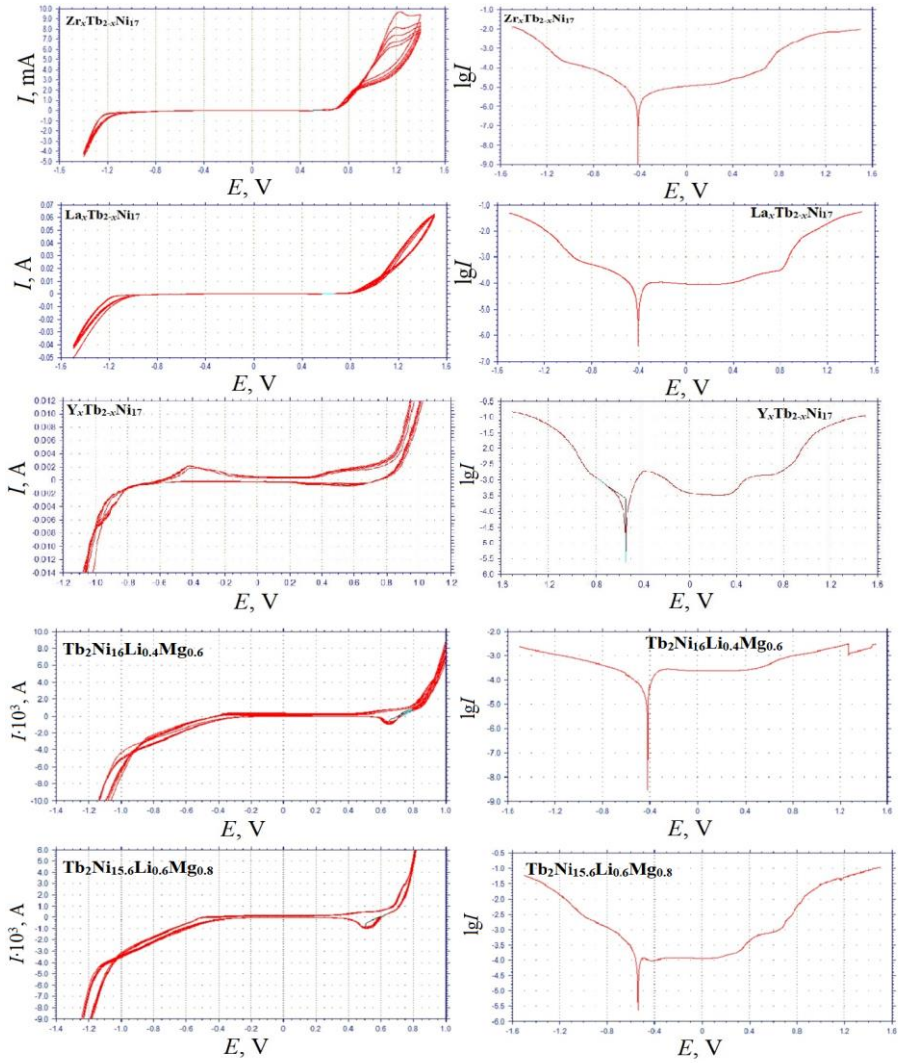

Fig. 6. Cyclic voltammetry (left) and dynamic polarization (right) curves for the $R_xTb_{2-x}Ni_{17}$-based electrodes.

presented in Fig. 7. All intermetallic samples show typical electrochemical behaviour. First area is connected with resistance of electrolyte, second (semicircle) is explained as kinetic and diffusion processes on the surface of the material. The last region shows the H-diffusion in the volume of solid state phase. The electrode based on the $Y_{0.5}Tb_{1.5}Ni_{17}$ showed two semicircles (small and large). First small semicircle explains electrochemical ability of the Ni-based phase $Y_{1.1(8)}Tb_{3.7(6)}Ni_{95.2(6)}$ (see Fig. 3). Large semicircle shows electrochemical processes of the main phase with 2:17 stoichiometry.

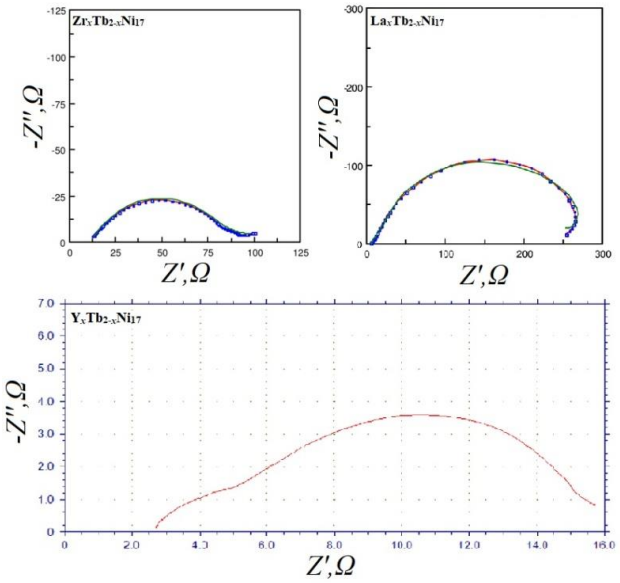

Fig. 7. Electrochemical impedance spectroscopy for the $R_xTb_{2-x}Ni_{17}$-based electrodes (Nyquist projections).

Conclusions

Alloys from $R_xTb_{2-x}Ni_{17}$ solid solutions were synthesized by arc-melting with further annealing at 400 ºC. The cell parameters of phases are: a = 8.2987(9) Å, c = 8.0206(8) Å, V = 478.37(9) Å^3 for $Zr_{0.5}Tb_{1.5}Ni_{17}$, a = 8.3161(6) Å, c = 8.0482(8) Å, V = 482.03(6) Å^3 for $Y_{0.5}Tb_{1.5}Ni_{17}$ and a = 8.3690(6) Å, c = 8.0560(7), V = 488.66(6) Å^3 for $La_{0.5}Tb_{1.5}Ni_{17}$. Under experimental condition capacity parameters are 1.81 H/f.u. for the Zr-containing electrode, 2.29 H/f.u. for the Y-containing electrode and 2.31 for the La-containing electrode. Hydrides can be interpreted as superstructures with the $Tb_2Mn_{17}C_{2.5}$-type (filled-up of the Th_2Ni_{17}-type). A corrosion stability of the electrodes in the alkaline electrolyte solution was studied by methods of X-ray phase analysis, scanning electron microscopy, energy-dispersive X-ray spectroscopy, cyclic voltammetry and electrochemical impedance spectroscopy. The $R_xTb_{2-x}Ni_{17}$ electrodes demonstrate good corrosion stability in alkaline solution. Potential corrosion for the $Y_{0.5}Tb_{1.5}Ni_{17}$-based electrode is -0.540 V, for $Zr_{0.5}Tb_{1.5}Ni_{17}$ – -0.413 V, for $La_{0.5}Tb_{1.5}Ni_{17}$ – -0.405 V, for $Tb_2Ni_{16.4}Li_{0.2}Mg_{0.4}$ -0.410 V, and $Tb_2Ni_{15.6}Li_{0.6}Mg_{0.8}$ -0.550 V.

Acknowledgments

This work was supported by National Research Foundation of Ukraine (2022.01/0064).

Kordan V. – PhD, Research Fellow;
Nytka V. – PhD student;
Tarasiuk I. – PhD, Research Fellow;
Kluziak K. – PhD student;
Pavlyuk V. – DSc, Professor.

[1] J.-M. Joubert, M. Latroche, R. Černý, R. C. Bowman, A. Percheron-Guégan, K. Yvon, *Crystallographic study of $LaNi_{5-x}Sn_x$ ($0.2 \le x \le 0.5$) compounds and their hydrides*, J. Alloys. Compd., 293–295, 124 (1999); https://doi.org/10.1016/S0925-8388(99)00311-4.

[2] F. Meli, A. Zuettel, L. Schlapbach, *Effect of silicon on the properties of AB_5-Based alloys for battery electrode application*, Z. Phys. Chem., 183(1–2), 371 (1994); https://doi.org/10.1524/zpch.1994.183.Part_1_2.371.

[3] I. Stetskiv, V. Kordan, I. Tarasiuk, V. Pavlyuk, *Synthesis, crystal structure and physical properties of the $TbCo_{4.5}Si_xLi_{0.5-x}$ solid solution*, Physics and Chemistry of Solid State, 22(3), 577 (2021); https://doi.org/10.15330/pcss.22.3.577-584.

[4] B. Rożdżyńska-Kiełbik, I. Stetskiv, V. Pavlyuk, A. Stetskiv, *$LaNi_{4.6}Zn_{0.4-x}Li_x$ ($x \le 0.2$) solid solution phases due to Li-doping*, Solid State Sci., 113, 106552 (2021); https://doi.org/10.1016/j.solidstatesciences.2021.106552.

[5] H. H. Van Mal, K. H. J. Buschow, A. R. Miedema, *Hydrogen absorption in $LaNi_5$ and related compounds: Experimental observations and their explanation*, J. Less. Common. Met., 35(1), 65 (1974); https://doi.org/10.1016/0022-5088(74)90146-5.

[6] W. Zhou, Zh. Ma, Ch. Wu, D. Zhu, L. Huang, Yu. Chen, *The mechanism of suppressing capacity degradation of high-Al AB_5-type hydrogen storage alloys at 60 °C*, Int. J. Hydrog. Energy, 41, 1801 (2016); https://doi.org/10.1016/j.ijhydene.2015.10.070.

[7] F. Meli, A. Zuettel, L. Schlapbach, *Surface and bulk properties of $LaNi_{5-x}Si_x$ alloys from the view point of battery applications*, J. Alloys. Compd., 190(1), 17 (1992); https://doi.org/10.1016/0925-8388(92)90167-8.

[8] N. O. Chorna, V. M. Kordan, A. M. Mykhailevych, O. Ya. Zelinska, A. V. Zelinskiy, K. Kluziak, R. Ya. Serkiz, V. V. Pavlyuk, *Electrochemical hydrogenation, lithiation and sodiation of the $GdFe_{2-x}M_x$ and $GdMn_{2-x}M_x$ intermetallics*, Voprosy khimii i khimicheskoi tekhnologii, 2, 139 (2021); https://doi.org/10.32434/0321-4095-2021-135-2-139-149.

[9] Yu. Liu, H. Yuan, M. Guo, M. Jiang, *Effect of Y element on cyclic stability of A_2B_7 -type La–Y–Ni-based hydrogen storage alloy*, Int. J. Hydrog. Energy, 44, 22064 (2019); http://doi.org/10.1016/j.ijhydene.2019.06.081.

[10] L. Wang, X. Zhang, Sh. Zhou, J. Xu, H. Yan, Qu. Luo, Qi. Li, *Effect of Al content on the structural and electrochemical properties of A_2B_7 type La–Y–Ni based hydrogen storage alloy*, Int. J. Hydrog. Energy, 45, 16677 (2020); http://doi.org/10.1016/j.ijhydene.2020.04.136.

[11] J. Liu, Sh. Zhu, H. Cheng, Zh. Zheng, Zh. Zhu, K. Yan, Sh. Han, *Enhanced cycling stability and high rate discharge ability of A_2B_7-type La–Mg–Ni-based alloys by in-situ formed $(La,Mg)_5Ni_{19}$ superlattice phase*, J. Alloys Compd., 777, 1087 (2019); https://doi.org/10.1016/j.jallcom.2018.11.094.

[12] V. Nytka, V. Kordan, A. Stetskiv, V. Pavlyuk, *$Tb_{2-x}Nd_xZn_{17-y}Ni_y$ (x = 0.5, y = 4.83): a new intermetallic with a maximum disordered structure and its hydrogen storage properties*, Acta Cryst., C79, 257 (2023); https://doi.org/10.1107/S2053229623004369.

[13] V. Pavlyuk, W. Ciesielski, N. Pavlyuk, D. Kulawik, M. Szyrej, B. Rozdzynska-Kielbik, V. Kordan, *Electrochemical hydrogenation of $Mg_{76}Li_{12}Al_{12}$ solid solution phase*, Ionics, 25(6), 2701 (2019); https://doi.org/10.1007/s11581-018-2743-8.

[14] V. Pavlyuk, W. Ciesielski, N. Pavlyuk, D. Kulawik, G. Kowalczyk, A. Balińska, M. Szyrej, B. Rozdzynska-Kielbik, A. Folentarska, V. Kordan, *Hydrogenation and structural properties of $Mg_{100-2x}Li_xAl_x$ (x=12) limited solid solution*, Mater. Chem. Phys., 223, 503 (2019); https://doi.org/10.1016/j.matchemphys.2018.11.007.

[15] K. Dutta, O. N. Srivastava, *Synthesis, structural characterization and hydrogenation behaviour of the new hydrogen storage composite alloy La_2Mg_{17}-x wt% $LaNi_5$*, J. Mater. Sci., 28, 3457 (1993), https://doi.org/10.1007/BF01159822.

[16] V. Kordan, V. Nytka, I. Tarasiuk, O. Zelinska, V. Pavlyuk, *Synthesis, crystal structure, and electrochemical hydrogenation of the $La_2Mg_{17-x}M_x$ (M = Ni, Sn, Sb) solid solutions*, Eur. J. Chem., 12(2), 197 (2021); https://doi.org/10.5155/eurjchem.12.2.197-203.2092.

[17] V. Nytka, V. Kordan, V. Pavlyuk, *$La_{3.65}Mg_{30}Sb_{1.07}$ as a disordered derivative of Th_2Ni_{17}-type structure*, Z. Krist.-New Cryst. St., 237(6), 1147 (2022); https://doi.org/10.1515/ncrs-2022-0411.

[18] N. Pavlyuk, V. Nytka, V. Kordan, V. Pavlyuk, *Crystal structure of the hydrogen storage active phase $La_{12}Mg_{46}LiMn$*, Z. Krist.-New Cryst. St., 238(6), 1223 (2023); https://doi.org/10.1515/ncrs-2023-0416.

[19] O. Isnard, S. Miraglia, J. L. Soubeyroux, D. Fruchart, A. Stergiou, *Neutron diffraction study of the structural and magnetic properties of the $R_2Fe_{17}H_x(D_x)$ ternary compounds (R = Ce, Nd and Ho)*, J. Less-Common Met., 162, 273 (1990); https://doi.org/10.1016/0022-5088(90)90343-I.

[20] A. Percheron-Guégan, C. Lartigue, J. C. Achard, P. Germi, F. Tasset, *Neutron and X-ray diffraction profile analyses and structure of $LaNi_5$, $LaNi_{5-x}Al_x$ and $LaNi_{5-x}Mn_x$ intermetallics and their hydrides (deuterides)*, J. Less. Common. Met., 74(1), 1 (1980); https://doi.org.10.1016/0022-5088(80)90063-6.

[21] V. M. Kordan, O. I. Zaremba, P. Yu. Demchenko, V. V. Pavlyuk, *Synthesis and electrochemical properties of $Li_yCa_xNd_{1-x}MnO_3$ solid solution*, Acta Phys. Pol. A., 114(4), 273 (2022); https://doi.org/10.12693/APhysPolA.141.273.

[22] V. Kordan, O. Zaremba, P. Demchenko, V. Pavlyuk, *Synthesis and electrochemical properties of $Li_yM_{1-x}Ca_xMnO_3$ (M = Pr, Eu) solid solutions*, Physics and Chemistry of Solid State, 23(4), 699 (2022); https://doi.org/10.15330/pcss.23.4.699-704.

[23] MTech. Retrieved from: http://chem.lnu.edu.ua/mtech/mtech.htm [in Ukrainian].

[24] W. Kraus, G. Nolze, PowderCell for Windows (Federal Institute for Materials Research and Testing, Berlin, 2000).

[25] D. Schwarzenbach, Program LATCON: refine lattice parameters. (University of Lausanne, Lausanne, 1966).

[26] J. Rodriguez-Carvajal, The Satellite Meeting on Powder Diffraction of the XV Congress of the IUCr (Toulouse, 1990), p. 127.

[27] V. Kordan, V. Nytka, G. Kovalczyk, A. Balinska, O. Zelinska, R. Serkiz, V. Pavlyuk, *Influence of doping elements on the electrochemical hydrogenation efficiency of Tb_2Ni_{17}-based phases*, Chem. Met. Alloys, 10(1/2), 61 (2017); https://doi.org/10.30970/cma10.0355.

В. Кордан[1], В. Нитка[1], І. Тарасюк[1], К. Клузяк[2], В. Павлюк[1,2]

Синтез і електрохімічне гідрування фаз $R_xTb_{2-x}Ni_{17}$ та $Tb_2Ni_{17-y}M_y$ (R = Y, Zr, La; M = Li, Mg)

[1]Львівський національний університет імені Івана Франка, Львів, Україна,
[2]Гуманітарно-природничий університет імені Яна Длугоша, Ченстохова, Польща, vasyl.kordan@lnu.edu.ua

Сплави з області існування твердих розчинів $R_xTb_{2-x}Ni_{17}$ та and $Tb_2Ni_{17-y}M_y$ були синтезовані методом електродугового сплавляння з подальшим відпалом за 400 ºС. Кількісний та якісний склад сплавів та порошків електродних матеріалів був визначений скануючою електронною мікроскопією та енергодисперсійною рентгенівською спектроскопією. Співвідношення Tb/*R*/Ni та Tb/Ni/Mg у зразках також було підтверджено рентген-флуоресцентною спектроскопією. Параметри комірок для тернарних фаз $R_xTb_{2-x}Ni_{17}$ (x = 0,5) становлять: a = 8,2987(9) Å, c = 8,0206(8) Å, V = 478,37(9) Å^3 для R = Zr, a = 8,3161(6) Å, c = 8,0482(8) Å, V = 482,03(6) Å^3 для R = Y, a = 8,3690(6) Å, c = 8,0560(7), V = 488,66(6) Å^3 для R = La. Атоми Tb частково заміщуються атомами Y, Zr та La через близьке значення атомних радіусів. За умов експерименту ємнісний параметр становить 1,81 H/ф.о. для Zr-вмісного електрода, 2,29 H/ф.о. для Y-вмісного електрода та 2,31 H/ф.о. для La-вмісного електрода. У випадку одночасного заміщення електродів Li та Mg ми простежували вміст гідрогену більший за 2,5 H/ф.о. Внаслідок гідрування параметри комірок Zr- і La-вмісних фаз ізотропно збільшуються. Синтезовані гідриди можна інтерпретувати як надструктури з типом $Tb_2Mn_{17}C_{2,5}$ (заповнений тип Th_2Ni_{17}). Корозійна стійкість електродів у лужному середовищі електроліту була досліджена методами рентгенофазового аналізу, скануючої електронної мікроскопії, енергодисперсійної рентгенівської спектроскопії, циклічної вольтамперометрії та електрохімічної імпедансної спектроскопії. Електрод на основі $Y_{0,5}Tb_{1,5}Ni_{17}$ демонструє потенціал корозії -0.540 В, електроди зі складом $Zr_{0,5}Tb_{1,5}Ni_{17}$ та $La_{0,5}Tb_{1,5}Ni_{17}$ характеризуються потенціалом корозії -0.413 В та -0.405 В, відповідно. Електроди, що містять одночасно Li- та Mg- демонструють потенціал корозії -0.410 В ($Tb_2Ni_{16.4}Li_{0.2}Mg_{0.4}$) та -0.550 В ($Tb_2Ni_{15.6}Li_{0.6}Mg_{0.8}$).

Ключові слова: рентгенівська дифракція порошку; скануюча електронна мікроскопія; структурний тип Th_2Ni_{17}; електрохімічні властивості; нікель металогідридний акумулятор.